Research Article | Vol. 26, No. 12 | 11 Jun 2018 | OPTICS EXPRESS 14879
Optics EXPRESS

Reconfigurable optical-microwave filter banks using thermo-optically tuned Bragg Mach-Zehnder devices

Richard A. Soref,[1] Francesco De Leonardis,[2] AND Vittorio M. N. Passaro[2,*]

[1]*Department of Engineering, The University of Massachusetts, Boston, Massachusetts, 02125 USA*
[2]*Photonics Research Group, Dipartimento di Ingegneria Elettrica e dell'Informazione, Politecnico di Bari, Via Edoardo Orabona n. 4, 70125 Bari, Italy*
[*]*vittorio.passaro@poliba.it*

Abstract: A new reconfigurable, tunable on-chip optical filter bank is proposed and analyzed for the silicon-on-insulator platform at the ~1550 nm wavelength. The waveguided bank is a cascade connection of 2 x 2 Mach-Zehnder interferometer (MZI) filters. An identical standing-wave resonator is situated in each MZI "arm." Using the thermo-optic (TO) effect to perturb this waveguide's index, the TO heater stripes provide continuous tuning of the filter by shifting the resonance smoothly along the wavelength axis. To reconfigure and program the cascade array, a broadband 2 x 2 MZI-related switch is inserted between adjacent filters. The novel TO switch, described here, can provide either single or double interconnection of 2 x 2 filters. The filter resonator is a new in-guide array of N closely coupled phase-shifted Bragg-grating resonators that provide one resonant spectral profile with 5 to 100 GHz bandwidth. The length of each grating cavity in the N group is chosen according to the Butterworth filter technique, and this gives high peak transmission for the composite. The predicted spectral profiles of a three-stage cascade show two-or-three peaks, or two-or-three notches with movable wavelength-locations as well as tunable wavelength-separations between those features. A tunable notch within a wider movable passband is also feasible. Potential applications include microwave photonics, wavelength-selective systems, optical spectroscopy and optical sensing.

OCIS codes: (230.4555) Coupled resonators; (250.6715) Switching; (130.7408) Wavelength filtering devices; (230.1480) Bragg reflectors.

References and links

1. W. Zhang and J. Yao, "Silicon-based integrated microwave photonics," IEEE J. Quantum Electron. **52**, 1–12 (2016).
2. Y. Xie, Z. Gen, L. Zhuang, M. Burla, C. Taddei, M. Hoekman, A. Leinse, C. G. H. Roeloffzen, K.-J. Boller, and A. J. Lowery, "Programmable optical processor chips: toward photonic RF filters with DSP-level flexibility and MHz-band selectivity," Nanophotonics **7**, 1–34 (2017).
3. J. Capmany and P. Muñoz, "Integrated microwave photonics for radio access networks," J. Lightwave Technol. **32**(16), 2849–2861 (2014).
4. C. Doerr, "Silicon photonic integration in telecommunications," Front. Phys. **3**, 7 (2015).
5. Y. Li, Y. Zhang, L. Zhang, and A. W. Poon, "Silicon and hybrid silicon photonic devices for intra-datacenter applications: state of the art and perspectives," Photon. Res. **3**(5), B10–B27 (2015).
6. D. Pérez, I. Gasulla, L. Crudgington, D. J. Thomson, A. Z. Khokhar, K. Li, W. Cao, G. Z. Mashanovich, and J. Capmany, "Multipurpose silicon photonics signal processor core," Nat. Commun. **8**(1), 636 (2017).
7. L. M. Zhuang, C. G. H. Roeloffzen, M. Hoekman, K.-J. Boller, and A. J. Lowery, "Programmable photonic signal processor chip for radiofrequency applications," Optica **2**(10), 854–859 (2015).
8. J. Carolan, C. Harrold, C. Sparrow, E. Martín-López, N. J. Russell, J. W. Silverstone, P. J. Shadbolt, N. Matsuda, M. Oguma, M. Itoh, G. D. Marshall, M. G. Thompson, J. C. Matthews, T. Hashimoto, J. L. O'Brien, and A. Laing, "Universal linear optics," Science **349**(6249), 711–716 (2015).
9. M. Burla, X. Wang, M. Li, L. Chrostowski, and J. Azaña, "Wideband dynamic microwave frequency identification system using a low-power ultracompact silicon photonic chip," Nat. Commun. **7**, 13004–13012 (2016).

#325057 https://doi.org/10.1364/OE.26.014879
Journal © 2018 Received 1 Mar 2018; revised 12 Apr 2018; accepted 16 Apr 2018; published 29 May 2018

Optics EXPRESS

10. F. Horst, W. M. J. Green, S. Assefa, S. M. Shank, Y. A. Vlasov, and B. J. Offrein, "Cascaded Mach-Zehnder wavelength filters in silicon photonics for low loss and flat pass-band WDM (de-)multiplexing," Opt. Express **21**(10), 11652–11658 (2013).
11. B. Guan, S. S. Djordjevic, N. K. Fontaine, L. Zhou, S. Ibrahim, R. P. Scott, D. J. Geisler, Z. Ding, and S. J. Ben Yoo, "CMOS Compatible Reconfigurable Silicon Photonic Lattice Filters Using Cascaded Unit Cells for RF-Photonic Processing," IEEE J. Sel. Top. Quantum Electron. **20**, 8202110 (2014).
12. L. Zhou, Q. Sun, L. Lu, and J. Chen, "Programmable universal microwave-photonic filter based on cascadeddual-ring assisted MZIs," in Proceedings of the SPIE Photonics West Conference, San Francisco (29 Jan 2018), paper 10536–52.
13. R. Soref, "Tutorial: Integrated- Photonic Switching Structures," APL Photonics **3**(2), 021101 (2018).
14. H. Zhou, C. Qiu, X. Jiang, Q. Zhu, Y. He, Y. Zhang, Y. Su, and R. Soref, "Compact, submilliwatt 2 x 2 silicon thermo-optic switch based on photonic crystal nanobeam cavities," Photon. Res. **5**(2), 108–112 (2017).
15. X. Jiang, H. Zhang, C. Qiu, Y. Zhang, Y. Su, and R. Soref, "Compact and power-efficient 2 x 2 thermo-optical switch based on the dual-nanobeam MZI," Optical Fiber Communication Conference, paper Th2A.7, San Diego, 25 March 2018.
16. R. Soref, "Resonant and slow-light 2 x 2 switches enabled by nanobeams and grating-assisted waveguides," Progress in Electromagnetics Research Symposium, invited paper IP5.9, St. Petersburg, Russia (2017).
17. R. Soref and J. Hendrickson, "Proposed ultralow-energy dual photonic-crystal nanobeam devices for on-chip N x N switching, logic, and wavelength multiplexing," Opt. Express **23**(25), 32582–32596 (2015).
18. J. R. Hendrickson, R. Soref, and R. Gibson, "Improved 2 × 2 Mach-Zehnder switching using coupled-resonator photonic-crystal nanobeams," Opt. Lett. **43**(2), 287–290 (2018).
19. R. Soref, J. R. Hendrickson, and J. Sweet, "Simulation of germanium nanobeam electro-optical 2 × 2 switches and 1 × 1 modulators for the 2 to 5 μm infrared region," Opt. Express **24**(9), 9369–9382 (2016).
20. V. Veerasubramanian, G. Beaudin, A. Giguère, B. Le Drogoff, V. Aimez, and A. G. Kirk, "Waveguide-coupled drop filters on SOI using quarter-wave shifted sidewalled grating resonators," Opt. Express **20**(14), 15983–15990 (2012).
21. A. D. Simard and S. LaRochelle, "Complex apodized Bragg grating filters without circulators in silicon-on-insulator," Opt. Express **23**(13), 16662–16675 (2015).
22. A. D. Simard and S. LaRochelle, "High Performance Narrow Bandpass Filters Based on Integrated Bragg Gratings in Silicon-on-Insulator," in Proceedings of OFC (2015), Tu3A.2.
23. S. LaRochelle and A. D. Simard, "Silicon Photonic Bragg Grating Devices," in Proceedings of OFC (2017), Th1G.3.
24. R. Soref, F. De Leonardis, and V. M. N. Passaro, Mach-Zehnder Crossbar Switching and Tunable Filtering Using N-coupled Waveguide Bragg Resonators (submitted).
25. R. Soref, F. De Leonardis, V. M. N. Passaro, "Tunable Optical-Microwave Filters Optimized for 100 MHz Resolution, Opt. Express (submitted).
26. Z. Chen, J. Flueckiger, X. Wang, F. Zhang, H. Yun, Z. Lu, M. Caverley, Y. Wang, N. A. F. Jaeger, and L. Chrostowski, "Spiral Bragg Grating Waveguides for TM Mode Silicon Photonics," Opt. Express **23**(19), 25295–25307 (2015).

1. Introduction

This theoretical modeling-and-simulation paper deals with a new kind of waveguided on-chip integrated-photonic network called the "reconfigurable cascaded-filter array"(RCFA)which is a type of optical filter bank. At the output ports of the bank, complex optical spectral profiles are available, and those profile shapes are readily tuned by means of thermo-optical (TO) heater strips deployed upon individual Mach-Zehnder interferometer (MZI) filters located within the bank. Some examples of these spectral profiles are two-or-three peaks or two-or-three notches having tunable wavelength spacings and tunable wavelength locations. Also feasible is a movable passband containing a tunable notch. The RCFA is constructed from 2 x 2 building-block filters and in this paper we have focused on a new type of building block which is an MZI in which each of two identical waveguided "arms" consists of several Bragg-grating resonantors that are closely coupled to each other within a strip channel to form one effective resonator. As discussed below, this allows Bragg engineering of "rectangle-like" filter profiles having very steep side walls (fast roll off) as desired for high performance optical-microwave applications. Another innovation here is the introduction of a broadband 2 x 2 switch between adjacent 2x2 building-block filters to attain programmable interconnection of filters. Thus the RCFA is a filter bank comprised of broad switches and tunable filters. Several independent input optical signals can be processed independently and simultaneously by a group of filter banks integrated side-by-side on the chip. The proposed

Optics EXPRESS

independent TO control of both switches and filters gives a relatively large (albeit slow) perturbation of a given waveguide's effective index Δn.

The broadband device offers many practical possibilities for reconfiguring the RCFA. To provide for the blocking of unused or unwanted optical-interconnection paths within the RCFA bank, we have proposed a novel broadband 2 x 2 switch that has seven possible switching states: cross and bar, along with five states that provide partial or complete path blocking. This 7-state device is made from three broadband elements as shown below. This device enables programming of the cascaded MZI-filter responses, making the bank suitable for applications such as filtering the microwave sideband(s) impressed upon an optical carrier by an RF optical-amplitude modulator [1–3]. Wavelength-multiplexed chips [4–8] can benefit from such filters. Other potential applications include RF spectrum analysis in the optical-microwave chip as well as measurement of the unknown frequency of an RF input [9]. In addition, on-chip optical spectroscopy and optical sensing can be exploited with our RCFA structures. The photonics platform assumed here is the foundry-compatible and CMOS-compatible silicon-on-insulator (SOI) platform operating around 1550 nm.

The paper is organized as follows. After a background discussion, the device architecture and the numerical methods used to simulate the device behaviour under different operative conditions are presented in Section 3. Then, in Section 4, parametric simulations are reported for 2-cascaded MZIs and for 4 × 3and 1 × 3 x 4RFCA devices. Finally, Section 5 summarizes the conclusions.

2. Background discussion

Cascaded "fixed" filters made of unbalanced MZI have been reported [10].The prior art of reconfigurable integrated-photonic filter banks consists primarily of traveling-wave resonator structures, specifically a cascade of "ring assisted" MZIs which refers to a microring-resonator (MRR) side coupled to one or both connecting arms in each MZI. This arrangement gives effective results [11,12], however the MRR offers a series of resonances (not an individual resonance) and the MRR spectral profiles are Lorentzian, which is not ideal for sideband suppression. The alternative approach targeted here is the use of standing-wave resonators within each MZI arm. In that case, both reflected and transmitted spectra are present. However, the constructive and destructive interference that takes place within the MZI (in principle) sends all of the optical energy to the Drop and Through ports, with no light being reflected back to the Input port.

Several embodiments are available for the standing wave resonators–the several practical choices described in the switching tutorial [13]. Prominent among these are the nanobeam and the phase-shifted Bragg grating. The nanobeam air-hole lattice devices have received extensive coverage [14–19] that will not be amplified here. Regarding the grating-waveguide with its extended side teeth, several recent papers [20–23] have made an excellent start towards the use of Bragg resonant waveguides as fixed or "passive" filter devices. The goal in this work is to enlarge the Bragg MZI "competence" from passive uses to active tunable-filter applications.

Our recent analysis [24] found that "outer silicon teeth" were effective for engineering steep peaks with a phase-shifted grating resonator. Along one Si channel waveguide, a group of N such resonators can be strongly coupled with a grating-end separation of zero or π-radians (with zero favored in our work). We found that one composite resonator with very high transmission at its peak is formed, and the resulting narrowband profile has very fast roll-off. Having determined that, we calculated the performance of the N-coupled cavities in a 2 x 2 MZI cross-bar switch having the structure shown in Fig. 1 [24], where the multi-cavity effective index is changed identically in each arm by the TO heater stripe illustrated there.

Our next step is to change the emphasis of Fig.1 to the feasibility of optical filtering with continuous tuning. This amounts to using Fig. 1 in its "intermediate states" between cross and bar. We can use a number N of coupled cavities larger than that in Fig. 1 and get many

Optics EXPRESS

choices of filter shape. The length L_i of each grating cavity is a free parameter in our filter design. As explained in the recent paper [24], the Butterworth filter technique can be adopted for the choices of L_1—L_N, and this in turn yields very narrow 5-to-50 GHz 3-dB bandwidth, tunable, high-transmission profiles with steeper-than-Lorentzian sides. The footprint for $N \leqq 4$ is reasonably compact. We also explored the choice of wide-bandpass resonators in the MZI filter, and there we selected the apodized Hamming waveguide-Bragg-grating as the filter approach. Those Hamming filter devices are discussed in the sections below.

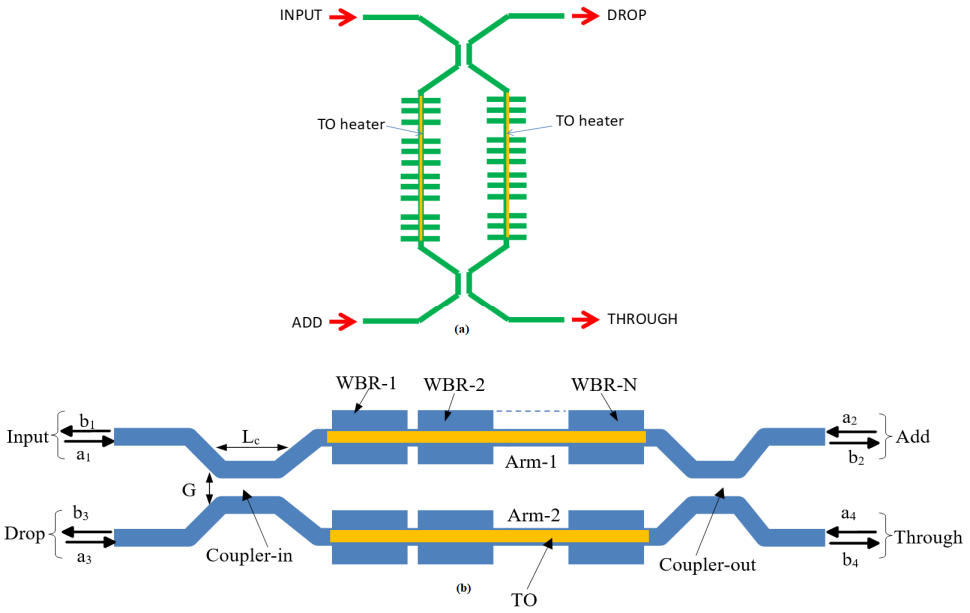

Fig. 1. (a) Schematic top view of TO-actuated 2 x 2 MZI crossbar switch in which each arm consists of two coupled Bragg-grating resonators; (b) Schematic top view of 2x2 MZI, showing the incoming and outcoming field amplitudes.

3. Device architecture and cascade-engineering method

When2 × 2 TO MZIs are connected in an optical series arrangement or "cascade", a variety of filter profiles becomes feasible at the cascade output ports as analyzed here. The simplest arrangement is two MZI filters connected as shown in Fig. 2(a) where the red box represents a broadband 7-states optical switch. A given single MZI filter has been chosen to contain either*N*-coupled waveguide Bragg resonators (WBRs), or Hamming-apodized waveguide Bragg gratings (WBGs).

We can engineer a specific spectral response for the N-coupled by designing opportunely the decay rates for each optical resonator. Hereafter, the Bragg section length of the first WBR is given as $LB_1 = M \times \Lambda$, where Λ,and M are the period length and the number of periods in the Bragg section of the first WBG. Moreover, the length of the *i-th* WBR (LB_i with $i \neq 1$) is expressed as a function of LB_1 in order to induce a maximally flat filter response [24]. Under the above-mentioned design conditions, the MZI is assumed symmetric having the WBRs of arm-1 and arm-2 matched at the same resonance wavelengths ($\lambda_1 = \lambda_2 = \lambda_0$) with both TO heaters Off.

In the case of the Hamming-apodized WBG, we have deliberately chosen for the Bragg structures silicon side-corrugations or "teeth" that protrude outside of the waveguide width.

Optics EXPRESS

Such teeth have a geometrical profile designed to induce the following Bragg coupling coefficient function:

$$\kappa_B(z) = \kappa_B^0 \left[0.54 - 0.46\cos\left(\frac{2\pi}{L_B} z \right) \right] \tag{1}$$

where κ_B^0 is the maximum coupling coefficient, while the terms L_B, and z represent the Bragg grating length and the coordinate along the propagation direction, respectively.

It is worth outlining that all MZIs considered here are physically realized on SOI strip waveguides covered by $SiO_2$and having width and height for single-mode operation. Moreover, the MZI Directional couplers (DCs), used as input and output devices, are designed to induce 3-dB behavior, and the tuning is actuated by TO heater strips deposited on the top of the WBRs or the Hamming WBGs.

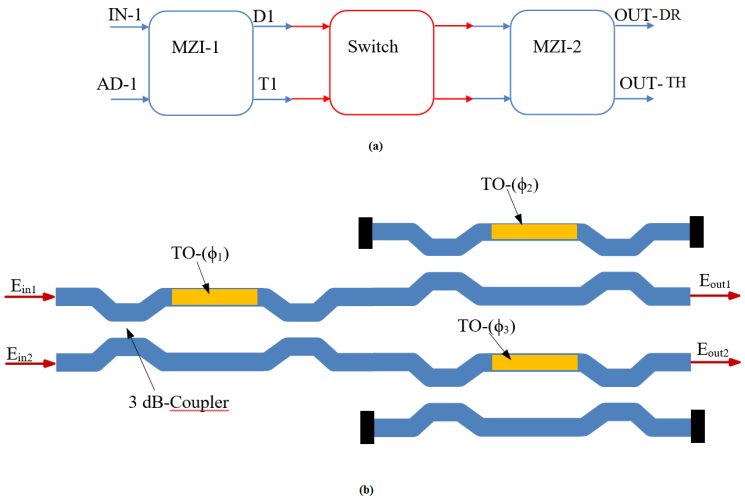

Fig. 2. (a) The 2-cascade of resonant 2 × 2 TO MZI building blocks, showing the middle seven states broadband optical switch (red box); (b) Architecture of the seven states broadband optical switch.

Figure 2(b) illustrates the proposed method of obtaining the seven states by joining a conventional broad MZI to a pair of broad conventional MZIs that have optical absorbers (shown in black) at two of their output ports. The idea is to make the pair function as two "terminated" 1 x 2 switches, where the terminated output gives blocking. As Fig. 2(b) shows, the TO heaters induce three independent values of phase shift named as ϕ_1, ϕ_2, and ϕ_3. Depending on the values of ϕ_i, with i = 1,2,3, the optical device assumes the following states of behavior: Block, Cross, Cross-upper, Cross-lower, Bar, Bar-upper, and Bar-lower. Indeed, with reference to the architecture of Fig. 2(b), the relationship between the input field amplitudes (E_{in1}, E_{in2}), and the output field amplitude (E_{out1}, E_{out2}) is given as in Eqs. (2)-(3):

$$E_{out1} = \left(-s^2 e^{-j\phi_2} + t^2 \right) \left(E_{in1} t^2 e^{-j\phi_1} - jE_{in2} s \cdot t e^{-j\phi_1} - jE_{in2} s \cdot t - s^2 E_{in1} \right) \tag{2}$$

$$E_{out2} = \left(t^2 e^{-j\phi_3} - s^2 \right) \left(-E_{in2} s^2 e^{-j\phi_1} - jE_{in1} s \cdot t e^{-j\phi_1} - jE_{in1} s \cdot t + t^2 E_{in2} \right) \tag{3}$$

Optics EXPRESS

where $s = -j\sqrt{k_c}$ and $s^2 + t^2 = 1$, with k_c the DC power coupling factor. Thus, assuming k_c = 0.5 (3-dB mechanism), we find the following behavior in Table 1. At this point a group of filter-MZIs can be interconnected into the form of particular mesh or array that includes some broadband crossbar switches. Figure 2(a) presents the simplest arrangement of this array.

Table 1. States of the broadband optical switch

STATES	Induced-phase shift			Output field Amplitude	
	ϕ_1 [rad]	ϕ_2 [rad]	ϕ_3 [rad]	E_{out1}	E_{out2}
Block	0	0	0	0	0
Cross	0	π	π	$-jE_{in2}$	jE_{in1}
Cross-upper	0	π	0	$-jE_{in2}$	0
Cross-lower	0	0	π	0	jE_{in1}
Bar	π	π	π	$-E_{in1}$	$-E_{in2}$
Bar-upper	π	π	0	$-E_{in1}$	0
Bar-lower	π	0	π	0	$-E_{in2}$

The Fig. 3(a) result is a multiple-signal optical processing network functioning as a programmable and reconfigurable optical filter bank. Now we shall generalize Fig. 3 to "higher order" filter banks. First we illustrate and propose in Fig. 3(a) a four-bank, three-cascade structure that we could designate as a 4 x 3 RCFA. Next, in Fig. 3(b), we look at one filter bank of Fig. 3(a) and show how we can expand the possible cascade output profiles by enlarging the MZI array in the second dimension. Therefore, the Fig. 3(b) bank, listed as 1 x 3 x 4, has added filter choices in its second and third stages. It is interesting that we could attach a broadband 8 x 1 switch to the eight ouput ports of this 1 x 3 x 4 and thereby obtain a single, selected output for this filter bank.

Determination of the RCFA output spectra is obtained using the transfer matrix approach. According to Eqs. (2)-(3), we can characterize the broadband crossbar switch-*kl* (the pair of indices *kl* represents the position of the switch inside the array [see Fig. 3] by means of the transfer matrix T_{Sw-kl}. Similarly using terms b_i and a_i to indicate the outcoming and the incoming field amplitudes at the generic MZI port (*i* = 1(2) for Input(Add) port, and *i* = 3(4) for Drop (Through), the 2 × 2 MZI-*mn* filter is fully described by Eq. (4):

$$\begin{bmatrix} b_2 \\ a_2 \\ b_4 \\ a_4 \end{bmatrix} = \boldsymbol{T}_{MZI-mn} \begin{bmatrix} b_1 \\ a_1 \\ b_3 \\ a_3 \end{bmatrix} = \begin{bmatrix} \boldsymbol{E}_{mn} & \boldsymbol{F}_{mn} \\ \boldsymbol{G}_{mn} & \boldsymbol{H}_{mn} \end{bmatrix} \begin{bmatrix} b_1 \\ a_1 \\ b_3 \\ a_3 \end{bmatrix} \tag{4}$$

where the $\boldsymbol{T}_{MZI-mn}$ is the 4 × 4 transfer matrix of the 2 × 2 MZI filter. The 2x2 matrices $\boldsymbol{E}_{mn}$, $\boldsymbol{F}_{mn}$, $\boldsymbol{G}_{mn}$ and $\boldsymbol{H}_{mn}$, are dependent upon the transfer matrices of the DCs and WBRs (or Hamming WBGs). The pair of indices *mn* represents the position of the MZI filter inside the array [see Fig. 3]. Therefore, the RCFA outputs are expressed as a particular matrix product between $\boldsymbol{T}_{MZI-mn}$ and $\boldsymbol{T}_{Sw-kl}$, depending on the array architecture. However, it is worth noting that the RCFA simulations are carried out by means of the implementation of a mixed numerical approach based on (1) the finite-element method (FEM), for the evaluation of the electric field distribution and overlap integrals, (2) the full vectorial coupled-mode theory (CMT) for the calculation of the optical features such as DC coupling factor and WBR (WBG) reflectivity and transmittivity, and (3) the transfer matrix for the system analysis.

Optics EXPRESS

4. Numerical results

The MZI filter cascades stemming from different states of the intervening broadband crossbar switches are investigated in this section. The wavelength of operation λ_0 is near 1550 nm, and the MZI filters are physically realized in a SOI wire waveguide having unperturbed cross section of $W = 450$ nm width and $H = 250$ nm thickness.

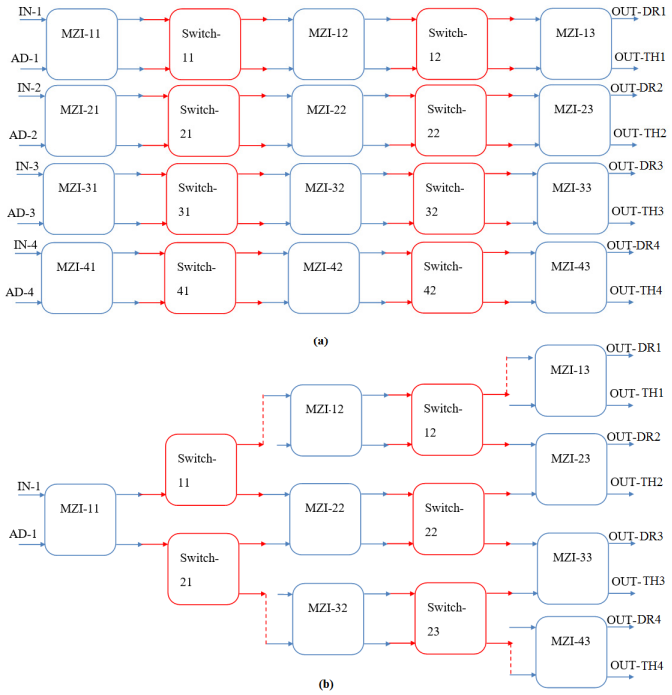

Fig. 3. (a) Four-bank Three-cascade RCFA;(b) One-bank, Three-cascade RCFA expanded laterally to four filters.

The Bragg grating sections are created by introducing along the nanowire, sidewall corrugations having a width extension (W_t) constant and equal to 100 nm, for the WBRs, while changing from 5 nm up to a maximum value of 50 nm to induce the Hamming apodization in the WBGs. The period is chosen to be $\Lambda = 315$ nm in order to operate at the central wavelength of 1550 nm. Hereafter, we focus the design and analysis on the TE polarization, specifically the TE_{00} fundamental optical mode. Moreover, as outlined in [24], the TO technique has been used as an efficient tool to induce refractive index changes (Δn) with low-power consumption. Indeed, the temperature increase required to obtain $\Delta n = 0.0015$ is about 8 K, due to silicon's thermo-optic coefficient $dn/dT = 1.86 \times 10^{-4}\ \mathrm{K}^{-1}$. The dT required to achieve $\Delta n = 0.004$ is not excessive and is also included below.

With the aim of showing the potential of the interconnection of MZI filters to achieve practical spectral profiles, we summarize in Table 2 the features of the different Types of MZI used to obtain the quantitative results presented below.

Before examining the spectral response of filter cascades, let us examine the optical properties of individual MZI filters in Table 2: types A, B, and C. Over a spectral range that is 100 nm wide, we have calculated the optical power and optical phase exiting the Through-port; then we determined the power and phase exiting the Drop port over the same wavelength range. The results are presented in Fig. 4(a)-4(d). Some side lobes can be seen in both the transmitted and reflected profiles. However, for many filtering applications,

Optics EXPRESS

especially those for processing microwave signals, the spectral range of interest is much narrower, such as 6-nm in width, and in those cases the side lobes do not have any influence. This is seen below.

Table 2. MZI-filter features utilized in this work

Type	MZI arms configuration	Bandwidth (BW) [nm]	Bandwidth (BW) [GHz]
Type-A	WBR: $N = 3;\ M = 18$	1.48	184.8
Type-B	WBR: $N = 4;\ M = 20$	0.77	96.2
Type-C	WBR: $N = 3;\ M = 30$	0.15	18.7
Type-D	Hamming WBG: $\kappa_B^0 = 2.019 \times 10^3\ \mathrm{cm}^{-1}$	33.3	4160

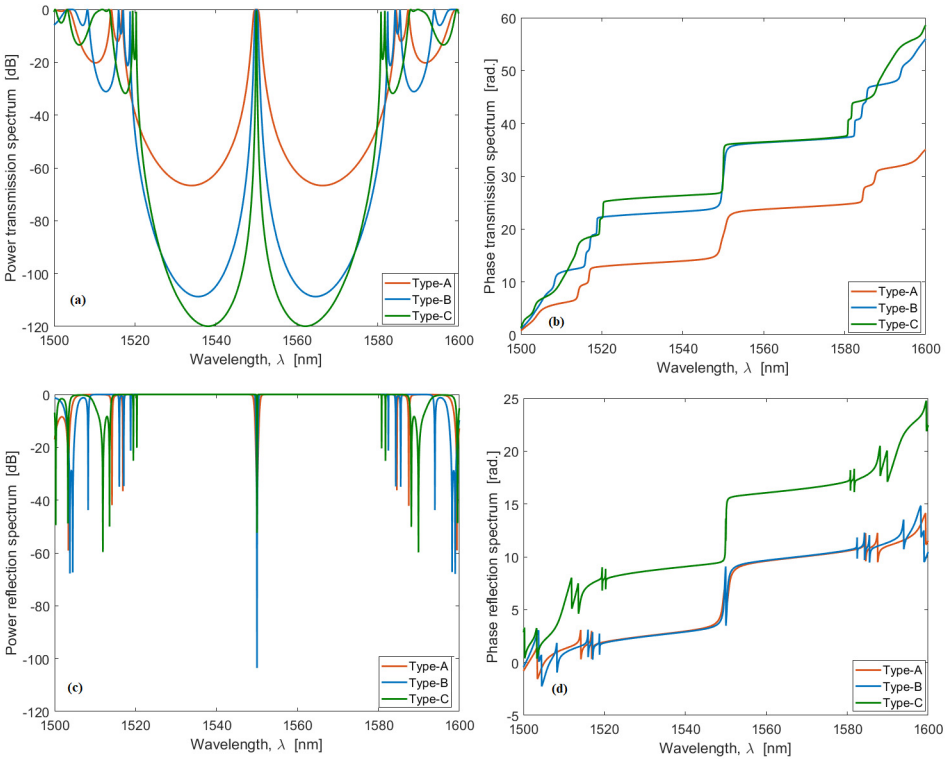

Fig. 4. Spectral features of different Types of WBR- MZI; (a) Power transmission spectrum; (b) Phase transmission spectrum; (c) Power reflection spectrum; (d) Phase reflection spectrum The simulations are performed by considering: W = 450 nm, H = 250 nm, W_t = 100 nm, α_l = 1dB/cm, assuming 1550 nm as the center resonance wavelength.

With reference to Fig. 2(a),the broadband crossbar switch is assumed to be in the Bar-lower state; and, as a result the Through signal of MZI-1($T1$) is addressed to the ADD input of MZI-2 (AD -2) as illustrated in Fig. 5. Then, the OUT-TH (Through spectrum) is plotted in Figs. 6(a)-6(b) for different values of the TO- induced refractive index changes (Δn_1 for MZI-1 and Δn_2 for MZI-2).

Optics EXPRESS

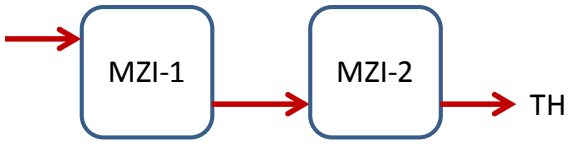

Fig. 5. Cascade interconnection for notch-in-band output profile.

Moreover in these simulations, we have considered MZI-1 and MZI-2 as Type-B and Type-C at the resonance wavelengths of 1551 nm and 1550.9 nm, respectively, and have taken the propagation loss coefficient (α_l) as 1 dB/cm.

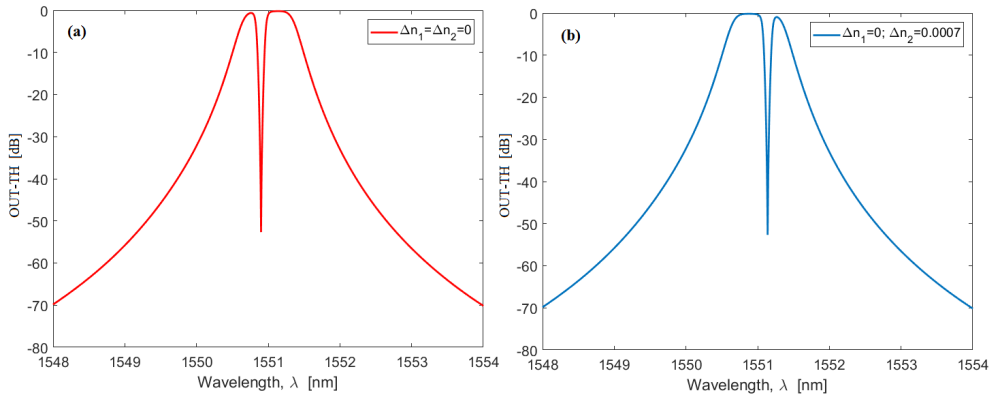

Fig. 6. Through spectra for 2-cascaded MZIs; (a)turning-Off TO_1 (Δn_1 = 0) and turning-Off TO_2(Δn_2 = 0); (b) turning-Off TO_1 (Δn_1 = 0) and switching-On TO_2 (Δn_2 = 0.0007);The simulations are performed by considering: W = 450 nm, H = 250 nm, W_t = 100 nm, α_l = 1dB/cm, MZI-1 = Type-B (at 1551 nm), MZI-2 = Type-C (at 1550.9 nm).

Figure 6 demonstrates the feasibility of a movable passband filter with a BW of 96.2 GHz, a low insertion loss less than −0.18 dB, and a tunable 18.7 GHz BW notch. Moreover, a notch red-shift of about 0.24 nm can be obtained by holding state TO_1 in the Off state and by switching-On TO_2. In addition, our data record a roll-off of about 39.4 dB/nm and 150.5 dB/nm for the bandpass filter and the notch, respectively.

Two notches with tunable spacings and wavelength locations can be realized by setting both MZI-1 and MZI-2 as Type-C MZIs having wavelengths resonance at 1550.0 nm and 1552.0 nm, respectively. The broadband crossbar switch is addressed in the Bar-upper state as is indicated in Fig. 7.

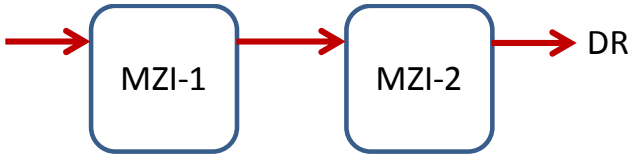

Fig. 7. Cascade interconnection for dual notch outputs.

In this context, Fig. 8 shows the OUT-DR (Drop spectrum) for different values of the TO-induced refractive index changes, Δn_1 , and Δn_2 .

Optics EXPRESS

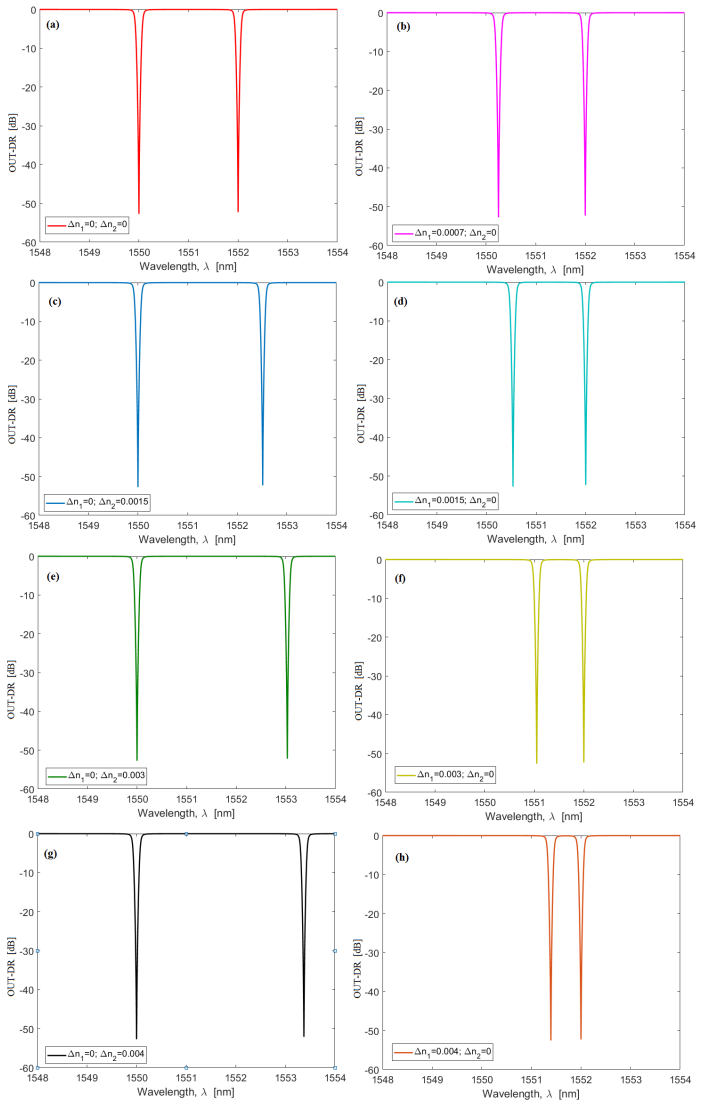

Fig. 8. Drop spectra for 2-cascaded MZI; (a) turning-Off TO_1 (Δn_1 = 0) and turning-Off TO_2(Δn_2 = 0); (b) switching-OnTO_1 (Δn_1 = 0.0007) and turning-Off TO_2 (Δn_2 = 0);(c) turning-Off TO_1 (Δn_1 = 0) and switching-On TO_2 (Δn_2 = 0.0015);(d) switching-On TO_1 (Δn_1 = 0.0015) andturning-OffTO_2 (Δn_2 = 0);(e) turning-Off TO_1 (Δn_1 = 0) and switching-On TO_2 (Δn_2 = 0.003);(f) switching-OnTO_1 (Δn_1 = 0.003) andturning-OffTO_2 (Δn_2 = 0);(g) turning-Off TO_1 (Δn_1 = 0) and switching-On TO_2 (Δn_2 = 0.004);(h) switching-OnTO_1 (Δn_1 = 0.004) and turning-Off TO_2 (Δn_2 = 0); The simulations are performed by considering: W = 450 nm, H = 250 nm, W_t = 100 nm, α_l = 1dB/cm, MZI-1 = Type-C (at 1550 nm), MZI-2 = Type-C (at 1552 nm).

The left panels show the tunability mechanism induced by the condition Δn_1 = 0 and $\Delta n_2 \neq 0$. As a result, an increasing of the notch spacing has been recorded. The opposite trend occurs when the operative condition $\Delta n_1 \neq 0$ and Δn_2 = 0, is addressed (see the right panels).

Optics EXPRESS

Thus, our simulations indicate that the separation between the notches can be tuned from 0.61 nm to 3.37 nm by switching-On TO_1 (Δn_1 = 0.004) and turning-Off TO_2, and by turning-Off TO_1 and switching-On TO_2 (Δn_2 = 0.004), respectively. Thus, a wavelength-shift of about 343.47 nm/RIU is induced by the thermo-optic Δn heater stripe formed on the top of each interferometer arm. The BW, the roll-off, and the insertion loss in Fig. 8 are18.7 GHz, 150.5 dB/nm, and –0.07 dB, respectively.

Some unique and perhaps unexpected results are found when two beams of filtered light are sent simultaneously into the Add and Input ports of the second MZI. Then an unusual addition of those two profiles occurs (rather than a multiplication) and the resulting output power spectrum of this second-stage MZI is governed by this physical law: $TH\left(MZI-2\right)=\left|d_1\times t_2+d_2\times t_1\right|^2$ where d_1 and t_1 are the amplitude spectrum exiting MZI-1 at its Drop port and Through ports, respectively, while t_2 and d_2 are the amplitude spectra of MZI-2 (Through and Drop) when that device has an Input consisting of a flat-spectrum. Taking the interconnection shown in Fig. 9, the novel feature of realizing two peaks can be obtained by setting the broadband crossbar switch in the Bar state.

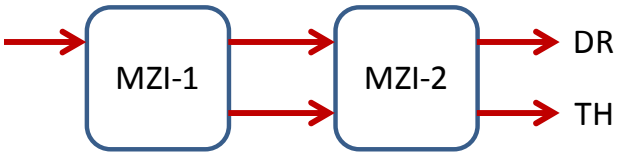

Fig. 9. Cascade interconnection for dual peaks or dual notches.

Under this configuration, the OUT-DR and OUT-TH shapes (Drop and Through) are shown in Fig. 10 by assuming MZI-1 and MZI-2 as Type-C MZIs with a roll-off of about 150.5 dB/nm, and having resonance wavelengths at 1550 nm and 1551 nm, respectively.

The OUT-TH plot reveals that the Bar state of the broadband switch induces two bandpass peaks (red curve) located at 1550 nm and 1551 nm, under the operative condition Δn_1 = 0 and Δn_2 = 0. Moreover, the second peak is red-shifted by 1.37 nm by turning-Off TO_1 and switching-On TO_2 (Δn_2 = 0.004), respectively. Moreover, the simulations indicate an insertion loss of –0.49 dB for the OUT-TH spectrum, and a BW of 19.7 GHz for the notch spectrum, recorded at the OUT-DR port.

Regarding applications of the Fig. 10 behaviors, the OUT-DR spectra offer a filter with widely variable bandwidth in the wavelength range between the notches. The twin-peak response of the OUT-TH spectra has several applications. One example is the on-chip generation of a microwave signal. For that use, we have found recently [25] that a greatly reduced BW for each peak in the Fig. 10 Type-C cascade can be achieved by increasing M into the 45 to 54 range which gives BW in the 100 MHz to 1 GHz range with moderate insertion loss. In that case, the Fig. 9 interconnection becomes a true optical-microwave filter with the above-mentioned ”signal” application, which is achieved by simultaneous narrow filtering of the left and right optical sidebands of an optical carrier that is input to MZI-1. Those sidebands are induced by DSB microwave modulation of the carrier. These selected left and right optical-transmission “slices” emerge together from the same output, MZI-2 TH, and are sent to a fast square-law photodetector that subsequently generates an optical-frequency-difference output between the two optical slices, a difference at RF baseband. This electrical output is a selected-frequency microwave signal.

Regarding the simulated passband insertion loss that is found for the cascades in Figs. 6, 8 and 10, that loss in dB is the sum of the MZI-stage losses, and an individual stage loss is proportional to the overall length L of the Bragg-grating structure in each arm of the MZI.

Optics EXPRESS

The specifics here for the Table 2 devices are: L = 37.0, 57.2 and 59.7 μm for Type A, B and C, respectively.

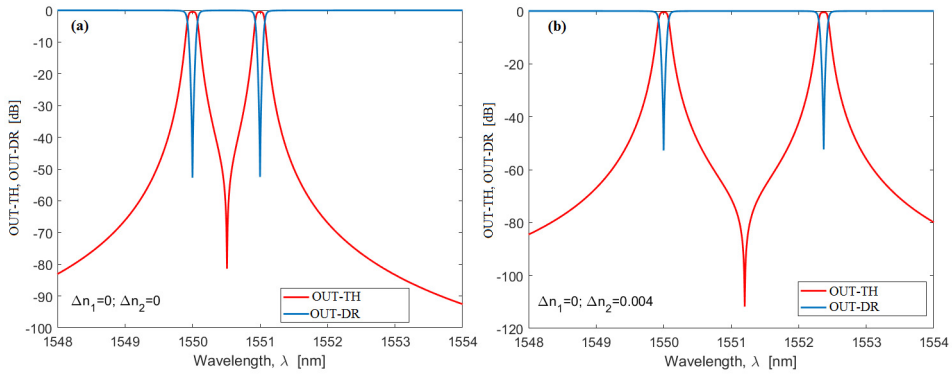

Fig. 10. Through and Drop spectra for 2-cascaded MZI; (a) turning-Off TO_1 (Δn_1 = 0) and turning-Off TO_2 (Δn_2 = 0); (b) turning-Off TO_1 (Δn_1 = 0) and switching-On TO_2 (Δn_2 = 0.004). The simulations are performed by considering: W = 450 nm, H = 250 nm, W_t = 100 nm, α_l = 1dB/cm, MZI-1 = Type-C (at 1550 nm), MZI-2 = Type-C (at 1551 nm).

Hence for our two-cascade, the total effective length is always less than 120 μm, and for that reason our simulation results are consistent with the experimental results of [26] where an SOI cm-scale spiral Bragg-grating waveguide with TE_{00} input at 1550 nm was measured to have 6 dB/cm loss including all factors such as radiation loss from the grating. Applying that result to our 120 μm case gives a predicted loss of 0.07 dB.

Considering now the case of a single grating-type resonator in each MZI arm, a broadband passband filter is achieved by combining two32-nm-BW Hamming-apodized WBGs sited at 1550 nm (MZI-1) and 1578nm (MZI-2), respectively. The sidewall corrugations width extension (W_t) have been changed in order to obtain a coupling factor $\kappa_B(z)$ satisfying Eq. (1). In this context, Fig. 11(a) shows the value of κ_B versus the corrugation width, as obtained by performing the overlap integrals by means of FEM simulations. At this step, the Hamming apodized Bragg grating profile can be deduced by Fig. 11(b), where the red curve indicates the teeth width W_t as a function of the number of periods distributed inside the Bragg grating length L_B. Moreover, in the plot of Fig. 11(b) we have assumed a tolerance δW_t = 5 nm, indicating that the corrugation width can change with a 5-nm step. As a result, the corrugation profile does not present a continuous shape shown by the black curve, where the ideal condition δW_t = 0 has been assumed.

Thus, under the design condition of Fig. 11(b) and by setting the crossbar switch in the Bar upper state as in Fig. 7, we obtain the curve of Fig. 11(c), where the OUT-DR is plotted as a function of the wavelength for different values of Δn_2, and assuming Δn_1 = 0. Our simulations indicate that a Bragg bandpass filter having a BW of about 7 nm can be obtained by turning-Off bothTO_1 and TO_2. Moreover, a BW tuning, a narrowing of about 1.05 nm and 1.78 nm was found by turning-OffTO_1, and switching-ON TO_2, with Δn_2 = 0.002, and 0.004, respectively. Moreover, setting MZI-2 initially at 1580 nm instead of 1578 nm, we record a BW reduction from 7 nm to 6.42 nm at the expense of an increase of the insertion loss from –0.09 dB to –0.343 dB, assuming turning-Off TO_1, and TO_2.

Let's return to the 4 x 3 RCFA of Fig. 3(a) and examine one example of what can be done. We launch four independent inputs and look at four independent Drop or Through outputs when we set the operating conditions that are listed in Table 3. The interesting aspect

Optics EXPRESS

here is that the 4 x 3 results presented in Figs. 12(a)-12(d) are those attained without any of the many possible TO tunings. In other words, all of the many TO heaters in Table 3 are assumed to be Off. The "initial condition" of Fig. 12 demonstrates the potential of realizing composite spectral profiles consisting of three notches [Fig. 12(a)] or three bandpass peaks [Fig. 12(b)] or twin notches in-band [Fig. 12(c)], or a notch within a Hamming-grating profile [Fig. 12(d)].

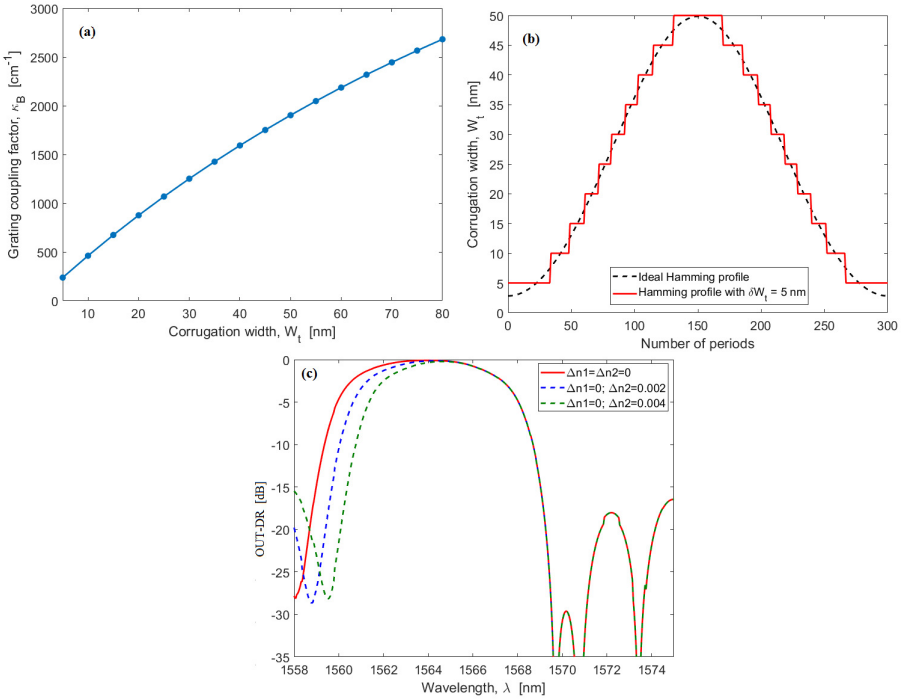

Fig. 11. (a) Grating coupling coefficient as a function of the corrugation width; (b) Hamming outside apodized Bragg grating profile. The black and red curves show the corrugation width profile in the ideal case (δW_t = 0), and δW_t = 5 nm of tolerance, respectively. (c) Drop spectra for 2-cascaded MZI for different values of Δn_2, assuming W = 50 nm, H = 250 nm, W_t = 100 nm, α_l = 1dB/cm, MZI-1 = Type-D (at 1550 nm), MZI-2 = Type-D (at 1578nm), and the crossbar switch in the Bar-upper state.

Regarding the feasible TO tunings in Figs. 12(a) and 12(b), we have simulated them, and the results (not shown here) indicate that the notch or peak spacing can indeed experience a wavelength shift of 343.47 nm/RIU induced by heater stripes. For Fig. 12(c),the narrow filter (BW = 184.8 GHz, and roll-off = 15.6dB/nm) is movable on the wavelength axis and the notches (BW = 18.7 GHz and roll-off = 150.5 dB/nm) can have their wavelength locations tuned. Similarly, the shapes in Fig. 11(d) can be translated along the wavelength axis. This 857.41-GHz-BW filter is obtained using an apodized-Hamming in stage 1 and in stage 2 together with a notch spectrum in stage 3. For each bank in Fig. 12, the necessary settings of the two broad 7-state switches are shown in Table 3.

Finally, we have investigated the behaviour of the expanded filter bank sketched in Fig. 3(b) where one input can produces eight outputs. It was found that the feasible filter shapes at the output ports were quite similar to those presented above in Figs. 6, 8, 10, 11 and 12. It was revealed that Fig. 3(b) offers a wide "repertoire" of useable filter profiles and the ability to rapidly reconfigure the bank using the five broadband switches shown in Fig. 3(b). Thus Fig. 3(b) can go from one group of output profiles to a different set.

Optics EXPRESS

If we consider the geometric features of the various filter banks discussed in this paper, we see that all of the constituent MZIs have nanometer-scale features that require high precision in the fabrication of the bank. In practice, there will always be fabrication errors related to dimensional inaccuracies in the MZI grating arms and coupler gaps. Such errors will give rise to unwanted increases in the IL and CT of stages and to unwanted reflections between stages.

Table 3. Illustrative example of Fig. 3(a) listing the operation conditions with all of the TO heaters Off

MZI-Type	Switch State	MZI-Type	Switch State	MZI-Type
MZI-11: Type-C (λ_0 = 1550.0 nm)	Switch-11: Bar-upper	MZI-12: Type-C (λ_0 = 1552.0 nm)	Switch-12: Bar-upper	MZI-13: Type-C (λ_0 = 1554.0 nm)
MZI-21: Type-C (λ_0 = 1550.0 nm)	Switch-21: Bar	MZI-22: Type-C (λ_0 = 1551.0 nm)	Switch-22: Bar	MZI-23: Type-C (λ_0 = 1552.0 nm)
MZI-31: Type-A (λ_0 = 1551.0 nm)	Switch-31: Bar-lower	MZI-32: Type-C (λ_0 = 1550.8 nm)	Switch-32: Bar-lower	MZI-33: Type-C (λ_0 = 1551.2 nm)
MZI-41: Type-D (λ_0 = 1550.0 nm)	Switch-41: Bar-upper	MZI-42: Type-D (λ_0 = 1578.0 nm)	Switch-42: Bar-upper	MZI-43: Type-C (λ_0 = 1564.0 nm)

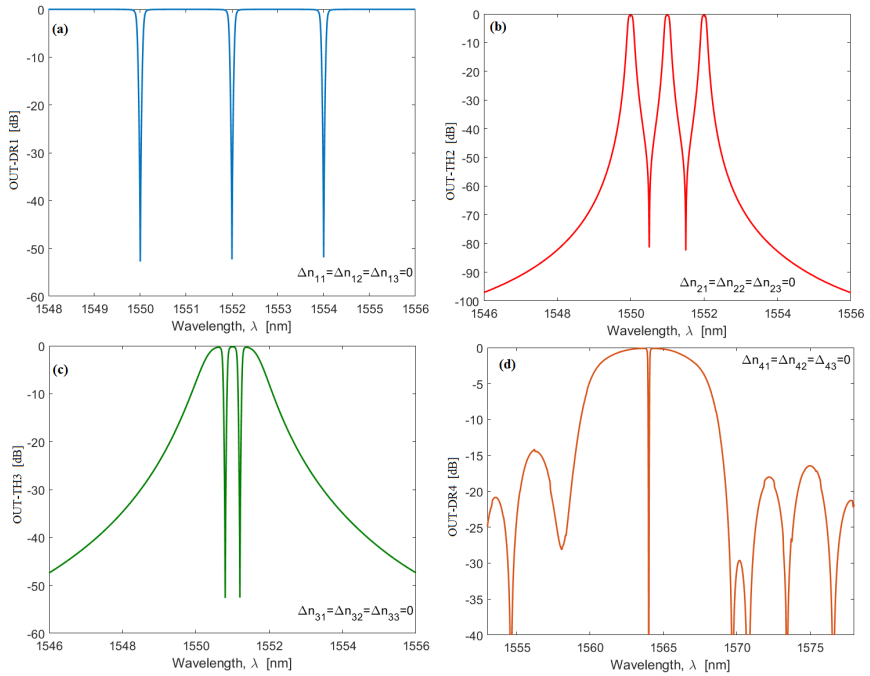

Fig. 12. Outputs of 4 × 4 RFCA, assuming all TOs in the Off state. Cases (a)-(d) of MZIs and the crossbar matrix switch are set as in Table 3.

The situation is similar to the N = 2 nanobeam case of [18] where an error analysis showed an increase of IL from −0.5 dB to −1.1 dB for mismatch of 0.06 nm between the resonance wavelengths of arm-1 and arm-2 in the MZI. The general solution to this problem, the way to minimize fabrication errors, is to manufacture the chip's filter bank in an advanced, high resolution, CMOS foundry. Even so, a few MZI errors would remain, however, their effect can be minimized. The approaches available to do this were discussed in [18]. The techniques include employing micron-scale direct-current TO heaters on the arms to "trim" their response on a constant basis, and/or to deposit atomic-layer dielectric films on the arms to offer permanent trimming of any imbalances.

Optics EXPRESS

5. Conclusions

In this paper, a novel on-chip filter bank and integrated arrays of banks were proposed and analyzed theoretically. The bank is a reconfigurable, programmable cascaded array of 2 x 2 MZI TO-tuned filters and 2 x 2 broadband MZI TO-actuated switches. Switches and filters are connected in alteration. The switches have seven states: cross and bar and five partially or fully blocked states. The seven states are attained from two terminated 1 x 2 MZIs joined to a conventional MZI. The filters are a new kind of waveguided Bragg-grating device in which each connecting arm of the integrated-photonic MZI consists of a novel standing-wave resonator. Continuous tuning arises from resonance shifting along the wavelength axis induced by waveguide-index perturbation. Each of two arms contains an identical "composite" high-transmission resonator comprised of N phase-shifted Bragg-grating resonators closely coupled to one another. Such MZI N-coupled filters have been analyzed using a "mixed" full-vectorial mathematical model based on finite-element modeling, coupled-mode theory and the transfer-matrix approach. The SOI platform, with SiO_2 upper cladding has been studied at the ~1550 nm wavelength.

Within the N-group of coupled resonators, the individual-cavity grating lengths have been chosen to satisfy the Butterworth filter technique, resulting here in a "rectangle-like" filter profile with high peak transmission, 5-to-100 GHz bandwidth, and very steep side walls having faster-than -Lorentzian roll-off. Gratings are constructed by extending numerous silicon "teeth" laterally beyond the 450-nm width of the silicon single-mode strip waveguide. For wide bandpass applications, the grating teeth in one resonator are apodized according to the Hamming procedure, and the MZI has only one cavity per arm.

Our numerical investigations of the filter bank predict a wide repertoire of tunable filter spectral profiles; specifically for a three stage cascade, we can attain two or three narrow peaks or two or three narrow notches in which the wavelength location of peak or notch is tunable, and where the wavelength-separation between features is also tunable. In addition, a tunable notch can be placed within a wider passband, where this band is also movable. In addition, the Hamming approach provides tunable-width passbands. Filters can also be added an inline bank along-side the other filters, giving more degrees of freedom in the reconfiguration.

Potential applications of the filter banks are numerous and include microwave-photonic applications such as filtering of the optical sideband(s) impressed upon an optical carrier by microwave modulation of that carrier. Related uses include an on-chip RF spectrum analyzer and measurement of an unknown RF frequency applied to an on-chip light wave. Wavelength-multiplexed on-chip systems can benefit from the filters. We also foresee applications in on-chip optical spectrometers and optical sensors.

Funding

Fondo per il finanziamento delle attività base di ricerca (MIUR FFABR 2017); Air Force Office of Scientific Research (FA9550-17-1-0354).